Available online at www.sciencedirect.com
SCIENCE DIRECT®
Solar Energy xxx (2005) xxx–xxx
SOLAR ENERGY
www.elsevier.com/locate/solener

Improvement and validation of a model for photovoltaic array performance

W. De Soto, S.A. Klein *, W.A. Beckman

Solar Energy Laboratory, University of Wisconsin-Madison, 1500 Engineering Drive, Madison, WI 53706, USA

Received 20 December 2004; received in revised form 21 June 2005; accepted 21 June 2005

Communicated by: Associate Editor Arturo Morales-Acevedo

Abstract

Manufacturers of photovoltaic panels typically provide electrical parameters at only one operating condition. Photovoltaic panels operate over a large range of conditions so the manufacturer's information is not sufficient to determine their overall performance. Designers need a reliable tool to predict energy production from a photovoltaic panel under all conditions in order to make a sound decision on whether or not to incorporate this technology. A model to predict energy production has been developed by Sandia National Laboratory, but it requires input data that are normally not available from the manufacturer. The five-parameter model described in this paper uses data provided by the manufacturer, absorbed solar radiation and cell temperature together with semi-empirical equations, to predict the current–voltage curve. This paper indicates how the parameters of the five-parameter model are determined and compares predicted current–voltage curves with experimental data from a building integrated photovoltaic facility at the National Institute of Standards and Technology (NIST) for four different cell technologies (single crystalline, poly crystalline, silicon thin film, and triple-junction amorphous). The results obtained with the Sandia model are also shown. The predictions from the five-parameter model are shown to agree well with both the Sandia model results and the NIST measurements for all four cell types over a range of operating conditions. The five-parameter model is of interest because it requires only a small amount of input data available from the manufacturer and therefore it provides a valuable tool for energy prediction. The predictive capability could be improved if manufacturer's data included information at two radiation levels.

Keywords: Photovoltaic cells; PV cells; Performance; *I–V* curves; Prediction; Solar energy

1. Introduction

The electrical power output from a photovoltaic panel depends on the incident solar radiation, the cell temperature, the solar incidence angle and the load resistance. Manufacturers typically provide only limited operational data for photovoltaic panels, such as the open circuit voltage (V_{oc}), the short circuit current (I_{sc}), the maximum power current (I_{mp}) and voltage (V_{mp}), the temperature coefficients at open circuit voltage and short circuit current ($\beta_{V_{oc}}$ and $\alpha_{I_{sc}}$, respectively), and the nominal operating cell temperature (NOCT).

* Corresponding author. Tel.: +1 608 263 5626; fax: +1 608 262 8464/8469.
E-mail address: klein@engr.wisc.edu (S.A. Klein).

0038-092X/$ - see front matter © 2005 Published by Elsevier Ltd.
doi:10.1016/j.solener.2005.06.010

Nomenclature

a	ideality factor parameter defined as $a \equiv N_s n_I k T_c/q$ (eV)
a_{0-4}	coefficients for air mass modifier in Eq. (17)
a_{ref}	ideality factor parameter at SRC (eV)
AM	air mass
b_{0-5}	coefficients for incidence angle modifier in Eq. (13)
E_g	energy bandgap (eV)
$E_{g,T_{ref}}$	energy bandgap at reference temperature (1.121 eV for silicon) (eV)
G	total irradiance on horizontal surface (W/m^2)
G_b	beam component of total irradiance on horizontal surface (W/m^2)
G_d	diffuse component of total irradiance on horizontal surface (W/m^2)
G_{ref}	irradiance at SRC (1000 W/m^2) (W/m^2)
I	predicted current (A)
I_L	light current (A)
$I_{L,ref}$	light current at SRC (A)
I_{mp}	current at maximum power point (A)
$I_{mp,ref}$	current at maximum power point at SRC (A)
I_o	diode reverse saturation current (A)
$I_{o,ref}$	diode reverse saturation current at SRC (A)
$I_{sc,ref}$	short circuit current at SRC (A)
k	Boltzmann's constant (1.38066E–23 J/K) (J/K)
K	glazing extinction coefficient (1/m)
$K_{\tau\alpha}$	incidence angle modifier at beam incidence angle θ
$K_{\tau\alpha,d}$	incidence angle modifier for diffuse component
$K_{\tau\alpha,g}$	incidence angle modifier for ground reflected component
L	thickness of transparent cover (m)
M	air mass modifier
M_{ref}	air mass modifier at SRC and air mass 1.5
NOCT	nominal operating cell temperature (K)
n	refractive index
n_I	ideality factor
n_D	diode factor (in King's model)
N_s	number of cells in series
P	predicted power (W)
P_{mp}	maximum power (W)
q	electron charge (1.60218E–19 C) (C)
R_{beam}	ratio of beam radiation on tilted surface to that on a horizontal surface
R_s	series resistance (Ω)
$R_{s,ref}$	series resistance at SRC (Ω)
R_{sh}	shunt resistance (Ω)
$R_{sh,0}$	shunt resistance at zero absorbed radiation = 50($V_{oc,ref}/I_{sc,ref}$) (Ω)
$R_{sh,ref}$	shunt resistance at SRC (Ω)
S	total absorbed irradiance (W/m^2)
S_{ref}	total absorbed irradiance at SRC (W/m^2)
T_c	cell temperature (K)
$T_{c,ref}$	cell temperature at SRC (K)
V	assigned voltage (V)
V_{mp}	voltage at maximum power point (V)
$V_{mp,ref}$	voltage at maximum power point at SRC (V)
$V_{oc,ref}$	open circuit voltage at SRC (V)
$\alpha_{I_{mp}}$	temperature coefficient for maximum power current (A/K)
$\alpha_{I_{sc}}$	temperature coefficient for short circuit current (A/K)
β	slope of the panel (°)
$\beta_{V_{oc}}$	open voltage temperature coefficient (V/K)
ε	material band gap energy (eV)
θ	incidence angle, angle between the beam of light and the normal to the panel surface (°)
θ_r	angle of refraction (°)
ρ	ground reflectance factor
$\tau(\theta)$	transmittance of glazing system at angle θ

These data are available only at standard rating conditions (SRC), for which the irradiance is 1000 W/m^2 and the cell temperature (T_c) is 25 °C (except for the NOCT which is determined at 800 W/m^2 and an ambient temperature of 20 °C). These conditions produce high power output, but are rarely encountered in actual operation. The results of this study were obtained using panel performance at SRC. Accurate, reliable, and easy to apply methods for predicting the energy production of photovoltaic panels are needed to identify optimum photovoltaic systems. The model developed by King (2000) and King et al. (1998, 2004) accurately predicts energy production with an algebraically simple model, but it requires parameters that are normally not available from the manufacturer. A database of the model parameters for many different array types is provided by Sandia National Laboratories (2002). A model that uses the only data provided by manufacturers to predict energy production is presented in this paper.

2. The current–voltage relationship for a photovoltaic device

The electrical power available from a photovoltaic (PV) device can be modeled with the well known equiv-

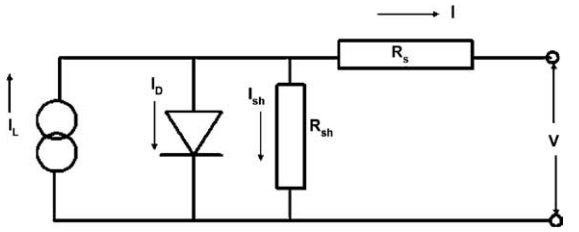

Fig. 1. Equivalent circuit representing the five-parameter model.

alent circuit shown in Fig. 1 (Duffie and Beckman, 1991; Nelson, 2003). This circuit includes a series resistance and a diode in parallel with a shunt resistance. This circuit can be used either for an individual cell, for a module consisting of several cells, or for an array consisting of several modules (Duffie and Beckman, 1991).

The current–voltage relationship at a fixed cell temperature and solar radiation for the circuit in Fig. 1 is expressed in Eq. (1). Five parameters must be known in order to determine the current and voltage, and thus the power delivered to the load. These are: the light current I_L, the diode reverse saturation current I_o, the series resistance R_s, the shunt resistance R_{sh}, and the modified ideality factor a defined in Eq. (2).

$$I = I_L - I_o\left[e^{\frac{V+IR_s}{a}} - 1\right] - \frac{V+IR_s}{R_{sh}} \quad (1)$$

where

$$a \equiv \frac{N_s n_I k T_c}{q} \quad (2)$$

The electron charge q, and Boltzmann's constant k are known, n_I is the usual ideality factor, N_s is the number of cells in series and T_c is the cell temperature. The power produced by the PV device is the product of the current and voltage.

Ideally, a PV panel would always operate at a voltage that produces maximum power. Such operation is possible, approximately, by using a maximum power point tracker (MPPT). Without an MPPT the PV panel operates at a point on the cell I–V curve that coincides with the I–V characteristic of the load. It is this second situation (i.e., no MPPT) that is the focus of this investigation.

2.1. The reference parameters

To evaluate the five parameters in Eq. (1), five independent pieces of information are needed. In general, these five parameters are functions of the solar radiation incident on the cell and cell temperature. Reference values of these parameters are determined for a specified operating condition such as SRC. Three current–voltage pairs are normally available from the manufacturer at SRC: the short circuit current, the open circuit voltage and the current and voltage at the maximum power point. A fourth piece of information results from recognizing that the derivative of the power at the maximum power point is zero. Although both the temperature coefficient of the open circuit voltage ($\beta_{V_{oc}}$) and the temperature coefficient of the short circuit current ($\alpha_{I_{sc}}$) are known, only $\beta_{V_{oc}}$ is used to find the five reference parameters. $\alpha_{I_{sc}}$ is used when the cell is operating at conditions other than reference conditions.

The five parameters appearing in Eq. (1) corresponding to operation at SRC are designated: a_{ref}, $I_{o,ref}$, $I_{L,ref}$, $R_{s,ref}$, and $R_{sh,ref}$. To determine the values of these parameters, the three known I–V pairs at SRC are substituted into Eq. (1) resulting in Eqs. (3)–(5).

For short circuit current: $I = I_{sc,ref}, V = 0$

$$I_{sc,ref} = I_{L,ref} - I_{o,ref}\left[e^{\frac{I_{sc,ref}R_{s,ref}}{a_{ref}}} - 1\right] - \frac{I_{sc,ref}R_{s,ref}}{R_{sh,ref}} \quad (3)$$

For open circuit voltage: $I = 0$, $V = V_{oc,ref}$

$$0 = I_{L,ref} - I_{o,ref}\left[e^{\frac{V_{oc,ref}}{a_{ref}}} - 1\right] - \frac{V_{oc,ref}}{R_{sh,ref}} \quad (4)$$

At the maximum power point: $I = I_{mp,ref}$, $V = V_{mp,ref}$

$$I_{mp,ref} = I_{L,ref} - I_{o,ref}\left[e^{\frac{V_{mp,ref}+I_{mp,ref}R_{s,ref}}{a_{ref}}} - 1\right] - \frac{V_{mp,ref}+I_{mp,ref}R_{s,ref}}{R_{sh,ref}} \quad (5)$$

The derivative with respect to power at the maximum power point is zero.

$$\left.\frac{d(IV)}{dV}\right|_{mp} = I_{mp} - V_{mp}\left.\frac{dI}{dV}\right|_{mp} = 0 \quad (6a)$$

where $dI/dV|_{mp}$ is given by

$$\left.\frac{dI}{dV}\right|_{mp} = \frac{\frac{-I_o}{a}e^{\frac{V_{mp}+I_{mp}R_s}{a}} - \frac{1}{R_{sh}}}{1 + \frac{I_o R_s}{a}e^{\frac{V_{mp}+I_{mp}R_s}{a}} + \frac{R_s}{R_{sh}}} \quad (6b)$$

The temperature coefficient of open circuit voltage is given by

$$\mu_{V_{oc}} = \left.\frac{\partial V}{\partial T}\right|_{I=0} \approx \frac{V_{oc,ref} - V_{oc,T_c}}{T_{ref} - T_c} \quad (7)$$

To evaluate $\mu_{V_{oc}}$ numerically, it is necessary to know V_{oc,T_c}, the open circuit voltage at some cell temperature near the reference temperature. The cell temperature used for this purpose is not critical since values of T_c ranging from 1 to 10 K above or below T_{ref} provide essentially the same result. V_{oc,T_c} can be found from Eq. (4) if the temperature dependencies for parameters

I_o, I_L, and a, are known. The shunt resistance, R_{sh} was assumed to be independent of temperature. Therefore, in order to apply Eq. (7), it is necessary to obtain expressions for the temperature dependence of the three parameters a, I_o and, I_L. The dependence of all of the parameters in the model on the operating conditions is considered in the following section.

2.2. Dependence of the parameters on operating conditions

From the definition of a, the modified ideality factor is a linear function of cell temperature (assuming n_I is independent of temperature) so that:

$$\frac{a}{a_{ref}} = \frac{T_c}{T_{c,ref}} \tag{8}$$

where $T_{c,ref}$ and a_{ref} are the cell temperature and modified ideality factor for reference conditions, while T_c and a are the cell temperature and modified ideality factor parameter for the new operating conditions.

Messenger and Ventre (2004) present an equation from diode theory for the diode reverse saturation current, I_o. The ratio of their equation at the new operating temperature to that at the reference temperature yields:

$$\frac{I_o}{I_{o,ref}} = \left[\frac{T_c}{T_{c,ref}}\right]^3 \exp\left[\frac{1}{k}\left(\frac{E_g}{T}\bigg|_{T_{ref}} - \frac{E_g}{T}\bigg|_{T_c}\right)\right] \tag{9}$$

where k is Boltzmann's constant and E_g is the material band gap. The values of the material band gap energies at 25 °C for the four cell types investigated in this study can be found in Table A.1. E_g exhibits a small temperature dependence (Van Zeghbroeck, 2004) which, for silicon, can be represented as indicated in Eq. (10) where $E_{g,T_{ref}} = 1.121$ eV for silicon cells. Eq. (10) was used for all of the cells considered in this study although the value of $E_{g,T_{ref}}$ used for the triple junction amorphous cell type was 1.6 eV.

$$\frac{E_g}{E_{g,T_{ref}}} = 1 - 0.0002677(T - T_{ref}) \tag{10}$$

The light current, (I_L), is nearly a linear function of incident solar radiation. Some pyranometers in fact use the short circuit current of a solar cell as a measure of the incident solar radiation. The light current (I_L) is observed to depend on the absorbed solar irradiance (S), the cell temperature (T_c), the short circuit current temperature coefficient ($\alpha_{I_{sc}}$), and the air mass modifier (M). The light current I_L for any operating conditions is related to the light current at reference conditions by

$$I_L = \frac{S}{S_{ref}}\frac{M}{M_{ref}}[I_{L,ref} + \alpha_{I_{sc}}(T_c - T_{c,ref})] \tag{11}$$

where S_{ref}, M_{ref}, $I_{L,ref}$, $T_{c,ref}$ are the parameters at reference conditions, while S, M, I_L, and T_c are the values for specified operating conditions. When using Eq. (11) to find the reference parameters, $S = S_{ref}$ and $M = M_{ref}$. The air mass modifier is assumed to be a function of the local zenith angle and is discussed below.

The information needed to determine the reference parameters is now complete. Eqs. (3)–(7) relate the model to the known reference conditions. To evaluate Eq. (7) it is necessary to included the temperature dependence of a, I_o and I_L as given by Eqs. (8)–(11). The simultaneous solution of these equations is facilitated with a non-linear equation solver, such as (Klein, 2005).

The final task to complete the model is to investigate the operating condition dependence of the series resistance R_s, and the shunt resistance, R_{sh}. The series resistance impacts the shape of current and voltage curve near the maximum power point. This effect is seen in Fig. 2 in which the current–voltage curves for the single-crystalline cell at SRC conditions have been plotted for series resistance values that are 20% greater and 20% lower than the value determined at reference conditions using Eqs. (1)–(11). The effect on the I–V curve is small and, although methods of adjusting R_s as a function of operating conditions have been investigated (De Soto, 2004), R_s is assumed constant at its reference value, $R_{s,ref}$ in this study.

The shunt resistance (R_{sh}) controls the slope of the I–V curve at the short circuit condition; large shunt resistances result in a horizontal slope. Fig. 3 shows the effect of halving and doubling the shunt resistance determined using Eqs. (1)–(11) for the single-crystalline cell at standard radiation conditions. The shunt resistance appears to change with absorbed solar radiation for all of the cells although the effect is most noticeable for cell types that have a relatively small shunt resistance at SRC, such as the triple junction amorphous cell. If experimental data were generally available at more than one solar radiation value, it would be possible to develop a rela-

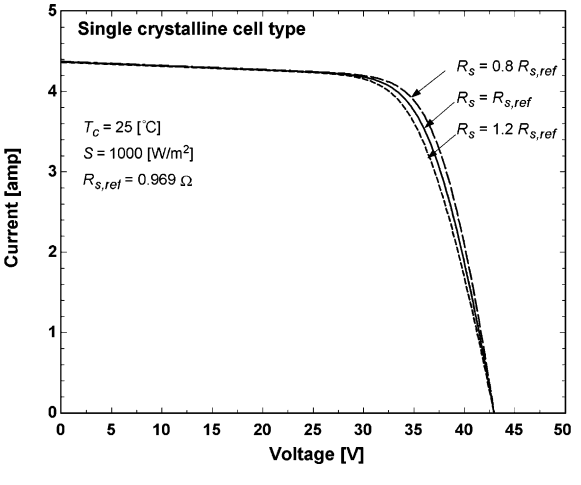

Fig. 2. Effect of series resistance for the single crystalline cell at standard rating conditions.

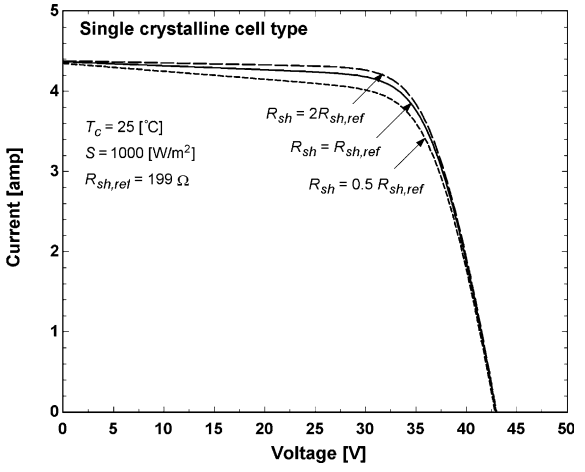

Fig. 3. Effect of shunt resistance for the single crystalline cell at standard rating conditions.

tion between the shunt resistance and absorbed radiation. However, this information is not normally available. Schroder (1998) indicates that the shunt resistance is approximately inversely proportional to the short-circuit current (and thus radiation) at very low light intensities. An observation apparent from an examination of the slopes of the I–V curves at short circuit conditions based on the experimental data from NIST is that the effective shunt resistance increases (and the slope thus decreases) as absorbed radiation is reduced. This behavior is observed for all cell types but it is most observable for the triple-junction amorphous cell type. Eq. (12), in which the shunt resistance is inversely proportional to absorbed radiation, is empirically proposed to describe this effect. The model specification is now complete.

$$\frac{R_{\mathrm{sh}}}{R_{\mathrm{sh,ref}}} = \frac{S_{\mathrm{ref}}}{S} \tag{12}$$

3. The incidence angle modifier, $K_{\tau\alpha}$

The incidence angle θ is the angle between the beam solar radiation and the normal to the panel surface. The incidence angle is directly involved in the determination of the radiation incident on the surface of the PV device. In addition, the incidence angle affects the amount of solar radiation transmitted through the protective cover and converted to electricity by the cell. As the incidence angle increases, the amount of radiation reflected from the cover increases. Significant effects of inclination occur at incidence angles greater than 65°.

The effect of reflection and absorption as a function of incidence angle is expressed in terms of the incidence angle modifier, $K_{\tau\alpha}(\theta)$ defined as the ratio of the radiation absorbed by the cell at some incidence angle θ divided by the radiation absorbed by the cell at normal incidence. The short circuit current is linearly dependent on the absorbed radiation. The incidence angle is dependent on the panel slope and location and on the time. Panels that are mounted on a vertical surface, for example, exacerbate the incidence angle effects because much of the annual beam solar radiation strikes the panel surface at angles greater than 65°. Nevertheless, vertically mounted panels are of interest because of the applicability of this orientation to installation on building façades. The experimental data that are available to validate the model presented in this paper were taken on a vertical surface.

King et al. (1998) provides a cell-specific correlation for the incidence angle modifier in the form shown in Eq. (13). Coefficients for many cell types have been determined by Sandia National Laboratories (2002). Coefficients for the PV modules tested by NIST were determined by Fanney et al. (2000b) and these coefficients are provided in Table A.1. However, an alternative form for $K_{\tau\alpha}(\theta)$ was developed for use with the five-parameter model that does not require specific experimental information.

$$K_{\tau\alpha}(\theta) = \sum_{i=0}^{5} b_i \theta^i \tag{13}$$

The incidence angle modifier for a PV panel differs somewhat from that of a flat-plate solar collector in that the glazing is bonded to the cell surface, thereby eliminating one air–glazing interface and the glazing surface may be treated so as to reduce reflection losses. Sjerps-Koomen et al. (1996) have shown that the transmission of this cover system can be well-represented by a simple air–glass model. Eqs. (14) and (15), based on Snell's and Bougher's laws as reported in Duffie and Beckman (1991), are used to calculate the incidence angle modifier for one glass–air interface. The angle of refraction (θ_r) is determined from Snell's law

$$\theta_r = \arcsin(n \sin\theta) \tag{14}$$

where θ is the incidence angle and n is an effective index of refraction of the cell cover. A good approximation of the transmittance of the cover system considering both reflective losses at the interface and absorption within the glazing is

$$\tau(\theta) = e^{-(KL/\cos\theta_r)}\left[1 - \frac{1}{2}\left(\frac{\sin^2(\theta_r - \theta)}{\sin^2(\theta_r + \theta)} + \frac{\tan^2(\theta_r - \theta)}{\tan^2(\theta_r + \theta)}\right)\right] \tag{15}$$

where K is the glazing extinction coefficient and L is the glazing thickness. In this study the value of K is assumed to be 4 m^{-1}, the value for "water white" glass and the glazing thickness is assumed to be 2 mm, a reasonable value for most PV cell panels. The refractive index is set to 1.526, the value for glass.

To obtain the incidence angle modifier ($K_{\tau\alpha}$), Eq. (15) needs be evaluated for incidence angles of 0° and θ. The ratio of these two transmittances yields the incidence angle modifier:

$$K_{\tau\alpha}(\theta) = \frac{\tau(\theta)}{\tau(0)} \tag{16}$$

Separate incidence angle modifiers are needed for beam, diffuse, and ground-reflected radiation, but each can be calculated in the same way. Average angles for isotropic diffuse and ground-reflected radiation are provided as a function of the slope of the panel by Fig. 5.4.1 of Duffie and Beckman (1991). Although these average angles for diffuse radiation were obtained for thermal collectors, they were found to yield reasonable results for PV systems.

A plot of the incidence angle modifier calculated using Eqs. (14)–(16) as a function of incidence angle is shown in Fig. 4. The incidence angle modifiers determined from Eq. (13) for the four cell types with the coefficients provided by Fanney et al. (2000b) are also shown in Fig. 4 with dotted lines. The plots are all similar. Differences are apparent at high incidence angles, but the incident radiation is normally low at these high angles and the uncertainty in the experimental values of the incidence angle modifier is larger at these conditions. The triple-junction amorphous cell type uses a thin polymer cover while the other three cell types employ a glass cover. The parameters for K, L and n used for glass are not likely not appropriate for the polymer cover, but the calculated cell performance for the conditions investigated was not found to be sensitive to these parameter values. The advantage of Eqs. (14)–(16) is that it eliminates the need for specific incidence angle modifier constants which are not generally available from the manufacturer. This method of estimating the incidence angle modifier is used in all of the following results for the five-parameter model.

4. The air mass modifier, M

Air mass is the ratio of the mass of air that the beam radiation has to traverse at any given time and location to the mass of air that the beam radiation would traverse if the sun were directly overhead. Selective absorption by species in the atmosphere causes the spectral content of irradiance to change, altering the spectral distribution of the radiation incident on the PV panel. King et al. (1998) developed an empirical relation to account for air mass:

$$\frac{M}{M_{\text{ref}}} = \sum_{0}^{4} a_i (\text{AM})^i \tag{17}$$

where AM is the air mass and is approximately given by King et al. (1998).

$$\text{AM} = \frac{1}{\cos(\theta_Z) + 0.5057(96.080 - \theta_z)^{-1.634}} \tag{18}$$

In Eq. (17) a_0, a_1, a_2, a_3, and a_4 are constants for different PV materials which are available for many cell types from Sandia National Laboratories (2002). These constants were also determined for the cells tested by NIST as reported by Fanney et al. (2002b). The NIST coefficients are listed for the four different cell types in Table A.1 and used to plot the air mass modifier as a function of zenith angle for the four cell types in Fig. 5. The air mass modifiers for the all cell types except the triple junction cell type are nearly the same for zenith angles between 0° and 75°. Zenith angles greater than 75° are generally associated with low solar radiation values and thus the differences observed in the air mass modifiers for large angles are not important. It was found that

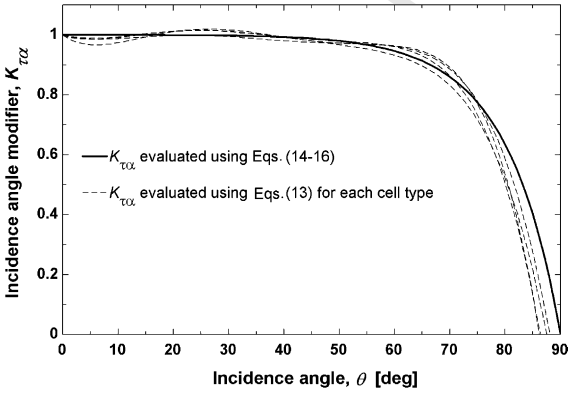

Fig. 4. Incidence angle modifier, $K_{\tau\alpha}$, as a function of incidence angle, θ, calculated using Eqs. (14)–(16) (solid line). The dotted lines are the incidence angle modifiers calculated using Eq. (13) with the coefficients for each cell type provided in Table A.1.

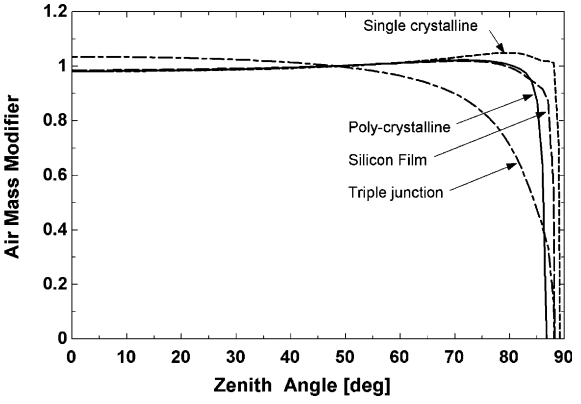

Fig. 5. Air mass modifier, M/M_{ref}, as a function of zenith angle, θ_z, calculated using Eq. (17) with the coefficients for each cell type listed in Table A.1.

if one set of air mass constants is chosen and used for all cell types there is little difference in the results compared to using a different air mass modifier relation for each cell type. Consequently, the air mass modifier for the poly-crystalline cell was used for all following results obtained with the five-parameter model.

5. Absorbed radiation, S

The major factor affecting the power output from a PV device is the solar radiation absorbed on the cell surface, S, which is a function of the incident radiation and the incidence angle. Radiation data are not normally known on the plane of the PV panel, so it is necessary to estimate the absorbed solar radiation using horizontal data and incidence angle information. The total absorbed irradiance S consists of beam, diffuse, and ground reflected components. Eq. (19) provides an approximate method of estimating the absorbed radiation, S, assuming that both diffuse and ground-reflected radiation are isotropic (Duffie and Beckman, 1991):

$$S = (\tau\alpha)_n \left[G_b R_{beam} K_{\tau\alpha,b} + G_d K_{\tau\alpha,d} \frac{(1+\cos\beta)}{2} + \rho K_{\tau\alpha,g} \frac{(1-\cos\beta)}{2} \right] \quad (19)$$

In Eq. (19), ρ is the ground reflectance, β is the slope of the panel, $K_{\tau\alpha,b}$ is the incidence angle modifier at the beam incidence angle, $K_{\tau\alpha,d}$ and $K_{\tau\alpha,g}$ are the incidence angle modifiers at effective incidence angles for isotropic diffuse and ground-reflected radiation, and R_{beam} is the ratio of beam radiation on a tilted surface to that on a horizontal surface.

The NIST data that were used to test the validity of the model included measurements of G_T, the solar radiation incident on the vertical PV array surface. However, the beam, diffuse and ground-reflected components were not measured so it was necessary to estimate these radiation components in order to determine the incidence angle modifiers in Eq. (19). Employing the same assumptions used for Eq. (19), the solar radiation on the array surface can be expressed as:

$$G_T = G_b R_{beam} + G_d \frac{(1+\cos\beta)}{2} + G_\rho \frac{(1-\cos\beta)}{2} \quad (20)$$

Values of G_T were available from the measurements on the vertical ($\beta = 90°$) surface. R_{beam} is a time dependent geometric factor provided in Duffie and Beckman (1991). The ground reflectance, ρ, was assumed to be 0.2. The only unknown in Eq. (19) is the diffuse fraction, G_d/G since $G_b = G - G_d$. The Erb's hourly diffuse fraction correlation (Duffie and Beckman, 1991) was used to estimate G_d/G as a function of the clearness index. Eq. (19) was solved to determine the clearness index and thus the total radiation and beam and diffuse components on a horizontal surface corresponding to the measured value of the radiation on the vertical surface.

Since the ratio of S/S_{ref} is needed for further calculations, Eq. (19) is more conveniently represented as:

$$\frac{S}{S_{ref}} = \frac{G_b}{G_{ref}} R_{beam} K_{\tau\alpha,b} + \frac{G_d}{G_{ref}} K_{\tau\alpha,d} \frac{(1+\cos\beta)}{2} + \frac{G}{G_{ref}} \rho K_{\tau\alpha,g} \frac{(1-\cos\beta)}{2} \quad (21)$$

where G_{ref} is the radiation at SRC conditions (1000 W/m^2) at normal incidence so that $(\tau\alpha)_n$ cancels out.

6. Validation of the five-parameter model

The data used for this study were provided by Fanney et al. (2002a) from a building integrated photovoltaic facility at the National Institute of Standards and Technology (NIST) in Gaithersburg, Maryland. The experimental data provide, at five-minute intervals, one year (1 January 2000–31 December 2000) of meteorological data, and measured cell temperatures along with current and voltage values for four different photovoltaic cell technology types installed on a vertical surface. The four different cell technologies are: single-crystalline, poly-crystalline, silicon thin film, and triple-junction amorphous.

The solid lines in Fig. 6 show typical results at 4 different operating conditions calculated for the single-crystalline cells with the five-parameter model presented in this paper. Also shown in Fig. 5 are the NIST experimental data (open circles) and the results obtained with the King model (closed circles). A summary of the King

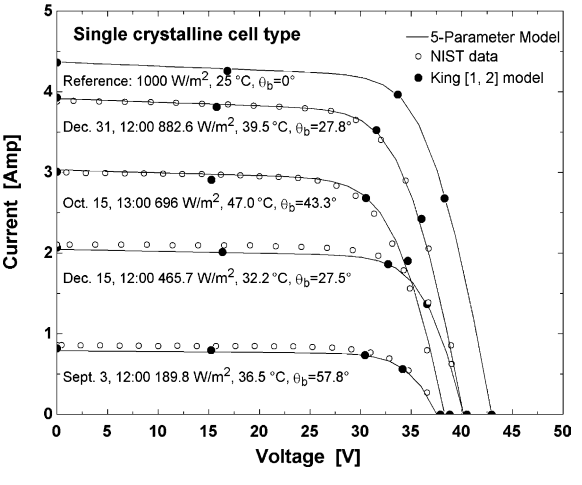

Fig. 6. Current vs voltage for the single-crystalline cell type predicted by the five-parameter model (solid lines), the King model (closed circles) and measured by NIST (open circles) for four operating conditions and the SRC condition (dotted line).

model is provided in Appendix. The maximum power values measured by NIST and determined by the King and five-parameter models at SRC conditions and at the 4 operating conditions are shown in Table 1. Figs. 7–9 and Tables 2–4 show similar information for the other three cell types. Note that the reference parameters for all four cell types were determined at the SRC operating condition, 1000 W/m^2 and 25 °C. Differences between the experimental data and the calculated values occur as a result of limitations in the cell model itself, as well as in the methods used to calculate absorbed radiation, incidence angle modifier and air mass modifier. In addition, there are uncertainties inherent in the experimental data.

Figs. 6–8 show excellent agreement between the current–voltages points determined by the five-parameter model and NIST data. The King model shows slightly better agreement with the data but this behavior is expected since the model requires many measurements

Table 1
Maximum power values from NIST measurements and the King and five-parameter models for the single-crystalline cell type

Solar [W/m^2]	Temperature [°C]	Maximum power [W/m^2]		
		NIST	King	Five-parameter
1000.0	25.0	133.4	133.4	133.4
882.6	39.5	109.5	111.4	110.6
696.0	47.0	80.1	82.0	82.4
465.7	32.2	62.7	61.1	61.0
189.8	36.5	23.8	22.5	22.3

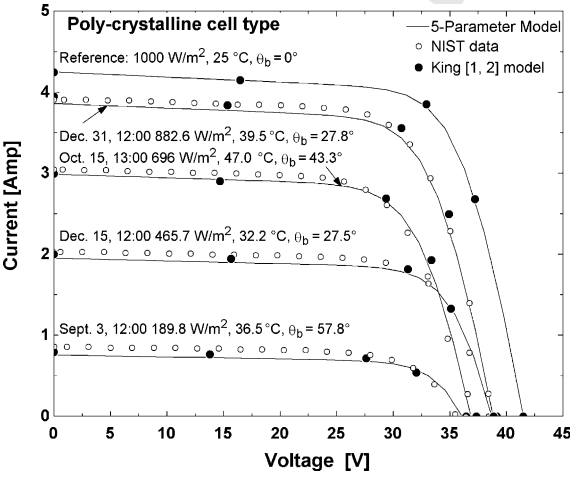

Fig. 7. Current vs voltage for the poly-crystalline cell type predicted by the five-parameter model (solid lines), the King model (closed circles) and measured by NIST (open circles) for four operating conditions and the SRC condition (dotted line).

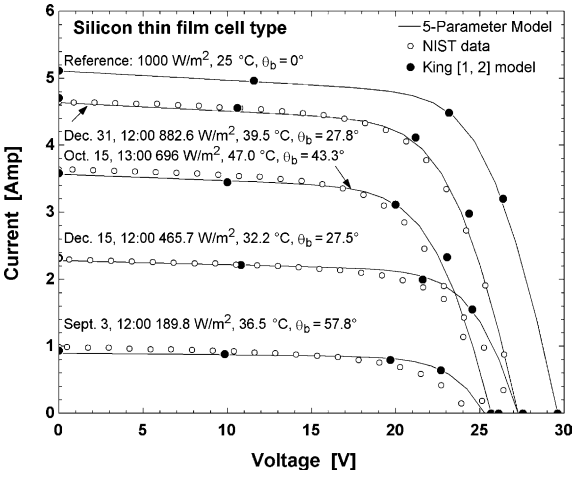

Fig. 8. Current vs voltage for the silicon thin film cell type predicted by the five-parameter model (solid lines), the King model (closed circles) and measured by NIST (open circles) for four operating conditions and the SRC condition (dotted line).

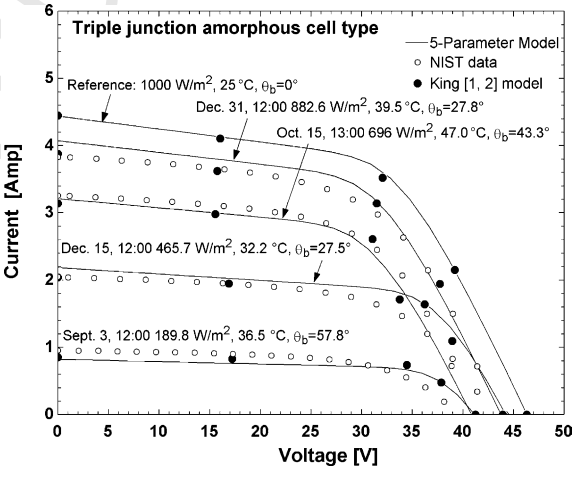

Fig. 9. Current vs voltage for the triple junction cell type predicted by the five-parameter model (solid lines), the King model (closed circles) and measured by NIST (open circles) for four operating conditions.

over a wide range of conditions to determine the model parameters. It is interesting to note that, at points where the experimental data and five-parameter results differ, such as the maximum power points for triple-junction cell in Fig. 9, the King model and five-parameter models tend to agree fairly well. The agreement could be improved if manufacturers were to provide two different I–V curves (one for low irradiance and one for high irradiance) instead of just one. The two curves could be used to generate an improved set of reference parameters (a_{ref}, $I_{L,ref}$, $I_{o,ref}$, $R_{s,ref}$, $R_{sh,ref}$).

Table 2
Maximum power values from NIST measurements and the King and five-parameter models for the poly-crystalline cell type

Solar [W/m^2]	Temperature [°C]	Maximum power [W/m^2]		
		NIST	King	Five-parameter
1000.0	25.0	125.8	125.8	125.8
882.6	39.5	106.8	109.3	105.6
696.0	47.0	77.4	79.1	78.1
465.7	32.2	56.6	56.9	55.8
189.8	36.5	21.2	18.5	20.6

Table 3
Maximum power values from NIST measurements and the King and five-parameter models for the silicon thin film cell type

Solar [W/m^2]	Temperature [°C]	Maximum power [W/m^2]		
		NIST	King	Five-parameter
1000.0	25.0	104.0	104.0	104.0
882.6	39.5	83.7	87.3	85.5
696.0	47.0	59.9	62.3	62.3
465.7	32.2	40.8	43.2	44.3
189.8	36.5	14.4	15.7	16.3

Table 4
Maximum power values from NIST measurements and the King and five-parameter models for the triple junction amorphous cell type

Solar [W/m^2]	Temperature [°C]	Maximum power [W/m^2]		
		NIST	King	Five-parameter
1000.0	25.0	115.8	115.8	115.8
882.6	39.5	94.2	98.9	100.8
696.0	47.0	78.5	81.2	76.8
465.7	32.2	51.7	57.8	61.2
189.8	36.5	22.6	25.4	22.0

7. Conclusion

The five-parameter model presented in this paper uses only data provided by the manufacturer with semi-empirical equations to predict the cell I–V curve (and thus the power) for any operating condition. The model requires a one-time calculation of the five parameters (a_{ref}, $I_{o,ref}$, $I_{L,ref}$, $R_{s,ref}$, and $R_{sh,ref}$) at reference conditions. These values are then used with in the model to calculate the parameters at other operating conditions, making it possible to predict the power output at any operating conditions. Comparisons with experimental data provided by NIST (Fanney et al., 2002a) have shown that the five-parameter model can be an accurate tool for the prediction of energy production for single-junction cell types. The five-parameter model uses only data provided by the manufacturer, and in contrast to King's model, does not require parameters that need to be predetermined by additional experiments. The predictions from the five-parameter model are shown to agree well with both the King model results and the NIST measurements for all four cell types over a range of operating conditions. The differences between the experimental data and the five-parameter model could be reduced if additional experimental data, e.g., I–V curves at two radiation levels, were used to determine the reference parameters.

Acknowledgements

We would like to thank the Graduate Engineering Research Students (GERS) for their financial support and Hunter Fanney and Mark Davis from the National Institute of Standards and Technology (NIST) for providing the data we used to validate the models. We especially wish to thank Mark Davis for his help and insight. We would also like to thank Michaël Kummert for his help in transforming the data to a convenient form.

Appendix. King's model

King's model shown in Eqs. (A.1)–(A.9), calculates the short circuit current (I_{sc}), current and voltage at the maximum power point (I_{mp} and V_{mp}, respectively), the currents at two intermediate points (I_x and I_{xx}), and the open circuit voltage (V_{oc}).

$$I_{sc} = I_{sc,ref}\left[\frac{M}{M_{ref}}\right][1 + \alpha_{I_{sc}}(T_c - T_{c,ref})]\left[\frac{G_b K_{\tau\alpha}(\theta) + G_d}{G_{ref}}\right] \quad (A.1)$$

$$I_{mp} = I_{mp,ref}[c_o E_e + c_1 E_e^2][1 + \alpha_{I_{mp}}(T_c - T_{c,ref})] \quad (A.2)$$

$$I_x = I_{x,ref}[c_4 E_e + c_5 E_e^2]\left[1 + \left(\frac{\alpha_{I_{sc}} + \alpha_{I_{mp}}}{2}\right)(T_c - T_{c,ref})\right] \quad (A.3)$$

$$I_{xx} = I_{xx,ref}[c_6 E_e + c_7 E_e^2][1 + \alpha_{1_{mp}}(T_c - T_{c,ref})] \quad (A.4)$$

$$V_{mp} = V_{mp,ref} + c_2 N_s \delta(T_c)\ln(E_e) + c_3 N_s[\delta(T_c)\ln(E_e)]^2 + \beta_{V_{mp}} E_e (T_c - T_{c,ref}) \quad (A.5)$$

$$V_{oc} = V_{oc,ref} + N_s \delta(T_c)\ln(E_e) + \beta_{V_{oc}} E_e (T_c - T_{c,ref}) \quad (A.6)$$

$$P_{mp} = I_{mp} V_{mp} \quad (A.7)$$

$$E_e = \frac{I_{sc}}{I_{sc,ref}[1 + \alpha_{I_{sc}}(T_c - T_{c,ref})]} \quad (A.8)$$

$$\delta(T_c) = \frac{n_D k T_c}{q} \quad (A.9)$$

Coefficients c_{0-7} and n_D, the diode factor, are given in Table A.1.

Table A.1
Values provided by NIST for the different cell types

Type of cell	Silicon thin film	Single-crystalline	Poly-crystalline	Three-junction amorphous
At reference conditions				
$P_{mp,ref}$ (W)	103.96	133.40	125.78	57.04
$I_{sc,ref}$ (A)	5.11	4.37	4.25	4.44
$V_{oc,ref}$ (V)	29.61	42.93	41.50	23.16
$I_{mp,ref}$ (A)	4.49	3.96	3.82	3.61
$V_{mp,ref}$ (V)	23.17	33.68	32.94	16.04
NOCT (K)	316.15	316.85	316.45	311.05
Temperature coefficients				
$\alpha_{I_{sc}}$ (A/K)	0.00468	0.00175	0.00238	0.00561
$\alpha_{I_{sc}}$ (1/K)	0.000916	0.000401	0.000560	0.001263
$\alpha_{I_{mp}}$ (A/K)	0.00160	−0.00154	0.00018	0.00735
$\alpha_{I_{mp}}$ (1/K)	0.000358	−0.000390	0.000047	0.002034
$\beta_{V_{oc}}$ (V/K)	−0.12995	−0.15237	−0.15280	−0.09310
$\beta_{V_{oc}}$ (1/K)	−0.004388	−0.003549	−0.003682	−0.004021
$\beta_{V_{mp}}$ (V/K)	−0.13039	−0.15358	−0.15912	−0.04773
β_{Vmp} (1/K)	−0.005629	−0.004560	−0.004830	−0.002976
King model parameters determined by NIST (Sjerps-Koomen et al., 1996) c_4–c_7 were obtained from Sandia http://www.sandia.gov/pv/docs/Database.htm				
a_0	0.938110	0.935823	0.918093	1.10044085
a_1	0.062191	0.054289	0.086257	−0.06142323
a_2	−0.015021	−0.008677	−0.024459	−0.00442732
a_3	0.001217	0.000527	0.002816	0.000631504
a_4	−0.000034	−0.000011	−0.000126	−1.9184E−05
b_0	0.998980	1.000341	0.998515	1.001845
b_1	−0.006098	−0.005557	−0.012122	−0.005648
b_2	8.117E−04	6.553E−04	1.440E−03	7.25E−04
b_3	−3.376E−05	−2.730E−05	−5.576E−05	−2.916E−05
b_4	5.647E−07	4.641E−07	8.779E−07	4.696E−07
b_5	−3.371E−09	−2.806E−09	−4.919E−09	−2.739E−09
c_0	0.9615	0.9995	1.0144	1.072
c_1	0.0368	0.0026	−0.0055	−0.098
c_2	0.2322	−0.5385	−0.3211	−1.8457
c_3	−9.4295	−21.4078	−30.2010	−5.1762
c_4	0.967	0.9980	0.9931	1.059
c_5	0.033	0.0020	0.0069	−0.059
c_6	1.12	1.159	1.104	1.188
c_7	−0.120	−0.159	−0.104	−0.188
n_D	1.357	1.026	1.025	3.09
Other parameters				
N_s	40	72	72	22
E_g (eV) at 25 °C	1.12	1.12	1.14	1.6

References

De Soto, W., 2004. Improvement and validation of a model for photovoltaic array performance. M.S. Thesis, Mechanical Engineering, University of Wisconsin-Madison.

Duffie, J.A., Beckman, W.A., 1991. Solar Engineering of Thermal Processes, second ed. John Wiley & Sons Inc., New York.

Fanney, A.H., Dougherty, B.P., Davis, M.W., 2002. Evaluating building integrated photovoltaic performance models. In: Proceedings of the 29th IEEE Photovoltaic Specialists Conference (PVSC), May 20–24, New Orleans, LA.

Fanney, A.H., Davis, M.W., Dougherty, B.P., 2002. Short-term characterization of building-integrated photovoltaic panels. In: Proceedings of the Solar Forum, Sunrise on the Reliable Energy Economy, ASES, Reno, NV, June 15–19.

King, D.L., 2000. Sandia's PV Module Electrical Performance Model (Version, 2000). Sandia National Laboratories, Albuquerque, NM, September 5.

King, D.L., Kratochvil, J.A., Boyson, W.E., Bower, W.I., 1998. Field Experience with a New Performance Characterization Procedure for Photovoltaic Arrays presented at the 2nd World Conference and Exhibition on Photovoltaic Solar energy Conversion, Vienna, Austria, July 6–10.

King, D.L., Boyson, W.E., Kratochvil, J.A., 2004. Photovoltaic array performance model, Sandia Report No. SAND2004-3535 available from US Department of Commerce, National Technical Information Service, 5285 Port Royal Rd, Springfield, VA 22161.

Klein, S., 2005. EES—Engineering Equation Solver, F-Chart Software, Available from: <www.fchart.com>.

Messenger, R.A., Ventre, J., 2004. Photovoltaic Systems Engineering, second ed. CRC Press LLC, Boca Raton, FL.

Nelson, J., 2003. The Physics of Solar Cells. Imperial College Press, London.

Sandia National Laboratories, 2002. Database of Photovoltaic Module Performance Parameters, Available from: <http://www.sandia.gov/pv/docs/Database.htm>.

Schroder, D.K., 1998. Semiconductor Material and Device Characterization, second ed. John Wiley & Sons Inc., New York.

Sjerps-Koomen, E.A., Alsema, EA., Turkemburg, W.C., 1996. A simple model for PV module reflection losses under field conditions. Solar Energy 57 (6), 421–432.

Van Zeghbroeck, B., 2004. Principles of Semiconductor Devices. Available from: <http://ece-www.colorado.edu/~bart/book/book/chapter2/ch2_3.htm>.